Heliyon 10 (2024) e35426

Contents lists available at ScienceDirect

Heliyon

journal homepage: www.cell.com/heliyon

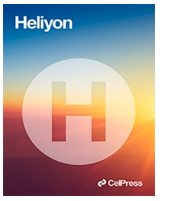

Research article

Multi-omics reveals protective effects of Ling Gui Zhu Gan Decoction on hyperlipidaemia in hamster

Baolin Li [a,b,c], Qi Qian [a,b,c], Liying Niu [a,b,c,*], Xinguo Wang [a,b,c,**]

[a] Hebei University of Chinese Medicine, Shijiazhuang, 050091, China
[b] Hebei Traditional Chinese Medicine Formula Granule Engineering & Technology Innovate Center, Shijiazhuang, 050091, China
[c] Quality Evaluation & Standardization Hebei Province Engineering Research Center of Traditional Chinese Medicine, Shijiazhuang, 050091, China

ARTICLE INFO

Keywords:
Ling Gui Zhu Gan decoction
Hyperlipidemia
Pharmacodynamics and mechanisms
Multi-omics
Differential metabolites and lipids

ABSTRACT

Ling Gui Zhu Gan decoction (LGZGD) is a traditional Chinese medicine (TCM) prescription that is widely used in cardiovascular disease clinical prevention and treatment with high efficacy. Recent studies have shown that LGZGD can also be used in hyperlipidemia (HL) intervention, but its pharmacodynamic material basis and its mechanisms remains unclear. This study aimed to reveal the protective effects of LGZGD on HL, elucidate the pharmacodynamic material basis. The hamster HL model was established by high-fat diet. Thereafter, non-targeted metabolomics and quantitative lipidomics were established for screening differential metabolites and pathways. Finally, the mechanisms were elucidated based on network pharmacology to screen for shared targets, which were computational selected by molecular docking. After four weeks of LGZGD administration, the TC, TG, and liver index levels decreased notably and hepatocyte injury was obviously reduced. The Multi-omics identified 62 differential metabolites and 144 differential lipids, respectively. The network pharmacology study predicted 343, 85, and 974 relevant targets from LGZGD components, HL, differential metabolites and lipids, respectively. Eventually, seven core targets were selected by molecular docking. Six key components in LGZGD, including genistein and naringenin, could play a therapeutic role in HL by regulating seven pathways, including HMGCR and PPARA. This comprehensive strategy provides a promising example and approach for further research on TCM for the treatment of lipid metabolic diseases.

1. Introduction

Recently, with the rapid development of the social economy and lifestyle improvement, hyperlipidemia (HL) has become a common disease and a serious threat to the health of millions of people worldwide [1]. The HL clinical manifestations are characterized by elevated serum levels of total cholesterol (TC) and triglycerides (TG), or reduced levels of high-density lipoprotein cholesterol, whose specific lipid profile alterations are well-established risk factors for the development of cardiovascular, atherosclerosis, coronary heart disease, and hepatic steatosis. Presently, the HL clinical treatment mainly involves statins, fibrates, ezetimibe, bile acid sequestrants, and niacin. However, their long-term application can cause adverse effects, including muscle toxicity, decreased liver functions, pancreatitis, venous thrombosis, and joint pain, which are detrimental to disease prevention and treatment [2–5].

* Corresponding author. No. 326, Xinshinan Road, Qiaoxi District, Shijiazhuang, Hebei Province, China.
** Corresponding author. Hebei University of Chinese Medicine, Shijiazhuang, 050091, China.
E-mail address: niuliyingyy@163.com (L. Niu).

https://doi.org/10.1016/j.heliyon.2024.e35426
Received 5 May 2024; Received in revised form 20 July 2024; Accepted 29 July 2024
Available online 8 August 2024

Therefore, further exploration of traditional Chinese medicine (TCM) prevention and treatment methods is required for safe and effective treatment with low side effects [6,7].

Ling Gui Zhu Gan decoction (LGZGD) is derived from Zhang Zhongjing's Synopsis of Golden Chamber, which indicates the LGZGD curative effects in case of phlegm in the heart or a chest fullness and vertigo sensation. In 2018, LGZGD was also listed in the first batch of the Catalogue of Ancient Famous Prescriptions by the National Administration of TCM. The prescription contains Fuling (dry sclerotia of *Poria cocos* (Schw.) Wolf, FL), Guizhi (dry twigs of *Cinnamomum cassia* Presl, GZ), Baizhu (dry rhizome of *Atractylodes macrocephala* Koidz., BZ) and Gancao (dry root and rhizome of *Glycyrrhiza uralensis* Fisch., *Glycyrrhiza inflata* Bat. or *Glycyrrhiza glabra* L., GC). LGZGD provides several therapeutic effects in heart failure, non-alcoholic fatty liver, obesity, and metabolic syndrome [8–11]. Previously, 149 LGZGD-related components were systematically characterized, and the contents of 20 components were simultaneously evaluated by UPLC–MS/MS (Tables S1–S2, Figs. S1–S2) [12]. Studies have shown that LGZGD can significantly decrease the liver and fat relative weights, TG, TC, low-density lipoprotein, and free fatty acid (FA) levels, which implies that LGZGD may serve as a therapeutic candidate for HL [13,14]. However, the pharmacodynamic material basis in regulating lipid metabolism have not been elucidated.

Metabolomics is a systematic approach to studying the variations of endogenous small molecule metabolites present in organisms at specific times and conditions. Screening of differential metabolites and inferring associated metabolic pathways contribute significantly to disease diagnosis and drug evaluation [15,16]. Lipidomics is an essential metabolomics branch that is used to comprehensively identify and quantify key lipid biomarkers relevant to disease or therapy. This can be highly helpful in the biological function analysis of different lipids, including energy metabolism, cell membrane function, signaling molecules and inflammatory response [17,18]. The integration of these two can provide a comprehensive and accurate assessment of the overall metabolic profiles, especially for the TCM multi-component and multi-target involvement in lipid metabolism regulation, which may positively contribute to drug efficacy and reveal the pharmacodynamic material basiss and mechanisms [19–21].

In order to comprehensively reveal the protective effects of LGZGD on HL, elucidate the pharmacodynamic material basis, a comprehensive approach was used (Fig. 1): step 1, animal experiments were performed to validate the LGZGD efficacy through physiological parameters after the HL hamster (HA) model was established using a high-fat diet. Step 2,the non-targeted metabolomics and quantitative lipidomics study were established for LGZGD against HL to screen for potential differential metabolites and lipids. Step 3, the potential targets of chemical components, HL, differential metabolites and lipids were predicted based on a network pharmacology approach, and the targets were used for screening key metabolic pathways for initial computational selection by molecular docking. Overall, this study provides a promising example and approach for further research on TCM for treating lipid metabolic diseases.

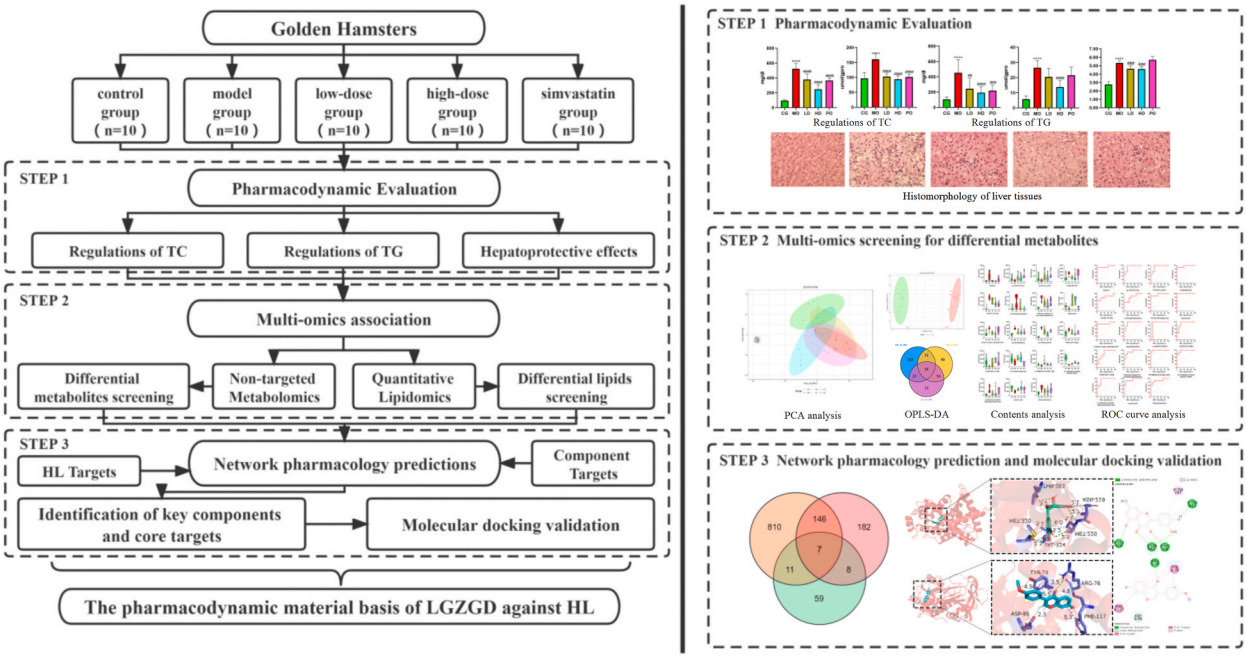

Fig. 1. Graphical abstract of the study.

2. Materials and methods

2.1. Chemicals and reagents

HPLC-grade methanol, acetonitrile, and isopropanol were purchased from Merck Co. (Darmstadt, Germany). Formic acid, 2-chlorophenyl alanine, ammonium formate, and chloroform were purchased from Thermo Fisher Co. (USA). Methyl tert-butyl ether was purchased from CNW Co. (Shanghai, China). Deionized water was purchased from Watson's™ Limited (Hong Kong, China). The assay kits of TC (batch number: AUZ3625) and TG (batch number: AUZ3592) were purchased from Beckman Coulter, Inc. (Suzhou, China).

2.2. Drug preparation

Botanical drugs (purchased from Hebei Jinnuokang Pharmaceutical Co.) included 55.2 g FL (batch number: YF18081902, source: Yunnan, China), 41.4 g GZ (batch number: 1710203, source: Guangxi-Guilin, China), 41.4 g BZ (batch number: YF18070702, source: Zhejiang, China) and 27.6 g GC (batch number: YF18063004, source: Neimeng, China). All the botanical drugs were mixed and boiled in 1200 mL purified water until 600 mL of the extracted solution remained, which was then filtered through a 200-mesh sieve and freeze-dried.

2.3. Animal experiments

HA, Male, weighing 140–160 g, were purchased from Hebei Invivo Biotechnology Co. (Production License: No. SCXK (JI) 2020-002).

The control group (CG) was fed a basal diet and the other groups were fed a high-fat diet (15 % fat, 0.5 % cholesterol, and 85 % basal diet). Water and food were replenished daily, and the experimental animals were kept in dry, clean, and ventilated living environments. After six weeks, the blood was collected from the orbital vein and the TC and TG serum levels were evaluated to determine whether the modeling was successful.

2.4. Animal grouping and drug administration

Fifty HA were randomly divided into five groups, namely CG, model group (MO), LGZGD low-dose group (clinical equivalent dose, LD), LGZGD high-dose group (two times clinical equivalent dose, HD), and simvastatin group (clinical equivalent dose, SG), with ten HA in each group.

The HA in the LD and HD were administered 2.5 g/kg/d and 5.0 g/kg/d, respectively. The SG were administered 1 mg/kg/d. The CG and MO were given equal amounts of distilled water by gavage once daily for four weeks. During the administration phase, 2 HA in MO and 1 in SG died, so that the final number of experimental animals in each group was 10 in CG, LD and HD, 9 in SG and 8 in MO.

2.5. Sample collection and processing

The blood was collected from the inner canthus using a serum collection tube. The samples were allowed to stand for 30 min and centrifuged (3000 rpm, 4 °C, 10min), which was taken as the serum samples.

The HA of all groups underwent fasting for 12 h from the time of the last administration and then, the blood was collected from the abdominal aorta after sodium pentobarbital anesthesia. The samples were immediately mixed upside down and centrifuged (3000 rpm, 4 °C, 10min), which was taken as the plasma samples.

Liver tissues were collected after blood sampling from the abdominal aorta. The livers were weighed and the liver index was calculated using the following formula: Liver index (%) = wet mass of liver/body weight × 100 %. Then, hematoxylin and eosin (HE) staining was performed to observe the pathomorphological changes in each group. Meanwhile, Liver tissues were harvested and washed with ice-cold saline to remove blood or debris. Samples were then finely minced and homogenized in PBS using homogenizer. The homogenate was centrifuged (5000 rpm, 4 °C, 10min) to separate the supernatant, which was used for the TG and TC kits, following the manufacturer's instructions.

2.6. Metabolomics analysis

2.6.1. Sample pre-processing

50 μL of the sample was added to 300 μL 20 % acetonitrile-methanol (1:4) extract, followed by vortexing (3min) and centrifuging (12000 rpm, 4 °C, 10min). Then, 200 μL of supernatant was allowed to stand 30 min (−20 °C) and centrifuged (12000 rpm, 4 °C, 3min), which was set aside for evaluation.

Meanwhile, 10 μL of each sample was aspirated from all samples, mixed, and used as quality control (QC) samples. The QC samples were tested after testing every ten samples to determine the stability of the instrument.

2.6.2. UPLC-Q-TOF-MS/MS conditions

A Shimadzu LC-20A UPLC liquid chromatography with Waters ACQUITY UPLC HSS T3 C18 (1.8 μm, 2.1 mm × 100 mm) column was used. The mobile phase was as follows: 0.1 % formic acid water (A)–0.1 % formic acid acetonitrile (B). The gradient elution

procedure was as follows: 0–11 min, 5%–90 % B; 11–12 min, 90 % B; 12–12.1 min, 90%–5% B; 12.1–14 min, 5 % B. The flow rate was as follows: 0.4 mL/min, column temperature: 40 °C, and injection volume: 2 μL.

An AB SCIEX Triple TOFTM 6600 with an electrospray ion (ESI) source was used for mass spectrometry. The samples were detected in both positive ion mode and negative ion mode in full scanning mode. The ion source temperature was 550 °C, GS1 50 psi, GS2 60 psi, CUR 35 psi, resolution 35000, and intensity threshold 500. The parent ion and fragment ion scanning ranges were *m/z* 50–1000 Da and *m/z* 25–1000 Da, respectively. In the positive and negative ion modes, the ion source voltage was 5.5 kV (ESI+) and −4.5 kV (ESI−), the declustering potential (DP) was 60 V (ESI+) and −60 V (ESI−), and the collision energy (CE) was 30 eV and CES 15 eV, respectively.

2.6.3. Data processing and multivariate statistical analysis

The raw LC-MS data were imported into ProteoWizard. The peak extraction, alignment, and retention time correction were performed using the XCMS program, and peak areas were corrected using the SVR method. The corrected peaks were compared with self-built databases, public libraries, and metDNA to identify metabolite information. The univariate and multivariate statistical analyses, including Student's t-test, principal component analysis (PCA), and orthogonal projections to latent structures discriminant analysis (OPLS-DA), were performed by R programs.

Based on this, metabolites with fold change (FC) $\geq$1.5 or FC $\leq$ 0.67, variable importance in projection (VIP) $\geq$1 and $P < 0.05$ were screened, followed by Venn diagrams, Kyoto Encyclopedia of Genes and Genomes (KEGG) database [22], metabolic pathway analyses to identify differential metabolites.

2.7. Lipidomics analysis

2.7.1. Sample pre-processing

50 μL of the sample was added to 1 mL lipid extract (3:1 methyl tert-butyl ether–methanol), followed by vortexing 2 min, sonicating 5 min, and then adding 200 μL water. After vortexing (1min) and centrifuging (12000 rpm, 4 °C, 10min), 200 μL of supernatant was concentrated and reconstituted with 200 μL lipid complex solution (1:1 acetonitrile–isopropanol) for detection. 10 μL of each sample was aspirated from all samples, mixed, and used as QC samples.

2.7.2. UPLC-Q-TOF-MS/MS conditions

AB SCIEX ExionLC™ AD UPLC liquid chromatography with Thermo Accucore™ C30 (2.6 μm, 2.1 mm × 100 mm i.d.) column was selected as the separation instrument. The mobile phase was as follows: A, acetonitrile/water (60/40, V/V) (containing 0.1 % formic acid, 10 mmol/L ammonium formate); B, acetonitrile/isopropanol (10/90, V/V) (0.1 % formic acid, 10 mmol/L ammonium formate). Gradient elution procedure: 0–2 min, 20%–30 % B; 2–4 min, 30–60 % B; 4–9 min, 60%–85 % B; 9–14 min, 85%–90 % B; 14–15.5 min, 90%–95 % B; 15.5–17.3 min, 95 % B; 17.3–17.5 min, 95%–20 % B; 17.5–20 min, 20 % B. The flow rate was 0.35 mL/min, the column temperature was 45 °C, and the injection volume was 2 μL.

AB SCIEX QTRAP 6500+ with the ESI source was used for mass spectrometry. The samples were detected in the MRM mode. The ion source temperature was 500 °C, GS1 45 psi, GS2 55 psi, CUR 35 psi, resolution 5000, and intensity threshold 1000. The ion source voltage in positive and negative ion modes was 5.5 kV (ESI+) and −4.5 kV (ESI−), respectively.

2.7.3. Data processing and multivariate statistical analysis

The raw LC-MS data were collected by Analyst Software 1.6.3 for peak identification, filtering, and quantitative analysis. Peaks with S/N < 5 and RT deviation >0.3 min were screened out and then sequenced by Multiquant 3.0.3. The final data was exported including information such as substance name, retention time, peak height, peak area, and substance concentration. The univariate and multivariate statistical analyses were performed by R programs, along with Student's t-test, PCA and OPLS-DA. Metabolites fulfilling both FC $\geq$ 2 or FC $\leq$ 0.5 and VIP $\geq$1 and $P < 0.05$ were screened.

2.8. Network pharmacology and molecular docking

The corresponding targets of 149 previously identified components were looked up with TCMSP and Swiss Target Prediction Database. HL targets were screened using Drugbank, GENECARD, OMMI and Therapeutic Target Database. Cytoscape software (version 3.8.2), KEGG database, human metabolome database and Swiss Target Prediction were applied for searching for the targets of differential metabolites and lipids. Eventually, the intersection targets of the three sections were selected for further computational selection.

Choosing potential pharmacological components and key targets for molecular docking. The crystal structures of the targets were downloaded from the PDB database to be saved in the PDB format. After removing the solvent and water using the PyMOL software, the targets were pre-treated by hydrogenation and charge calculation using AutoDockTools 1.5.6. Afterward, molecular docking was performed using AutoDock Vina (version 1.2.0), in which binding energy (<−5.0 kcal/mol) was selected as a basis for obtaining a reliable docking model.

3. Results

3.1. Regulations of TC and TG by LGZGD in HA with HL

Fig. 2A–D shows the serum and liver TC and TG levels. After modeling for six weeks, the TC and TG levels in MO, HD, LD, and SG were considerably significantly higher than those in CG, indicating successful HL modeling (Fig. S3). After four weeks of administration, the serum and liver TC and TG levels in HD decreased significantly compared with those in MO. The LD and SG also showed a similar downward trend, indicating that LGZGD could effectively decrease the TC and TG levels.

3.2. Hepatoprotective effects of LGZGD for the HA with HL

Compared with CG, the MO liver index increased significantly (Fig. 2E). Based on this, there was a distinct decrease in HD and LD, indicating that LGZGD has a certain therapeutic effect on HL. No significant difference was found in the liver index between SG and MO.

HE staining was performed to determine the LGZGD effects on the liver cell histomorphology. The CG hepatocytes were tightly arranged with no swelling or degeneration (Fig. 2F). The nuclei were mostly located in the center of the cells, which were regular in shape. The hepatocytes in MO were considerably enlarged and structurally disorganized, changing from polygonal to round and accompanied by balloon-like degeneration. In the LD, two hepatocyte degeneration forms were present, namely ballooning and turbid swelling. The HD liver tissue was more regular in structure, with only partial turbid swelling-like degeneration. Moreover, the SG hepatocytes were relatively well arranged.

3.3. Results of non-targeted metabolomics analysis

3.3.1. Results of multivariate statistical analysis

PCA was performed to visualize the separation trend, which was also used to determine the metabolic differences and the magnitude of variability within the groups. Fig. 3A and B shows the PCA score plots. In the positive ion mode, the CG showed distinct intra-group aggregation in the left upper region, whereas the MO was relatively discrete in the middle region, with significant differences between the two. Conversely, the HD and LD were clustered in the middle of the two, respectively. In the negative ion mode, the CG was relatively clustered in the upper middle region, whereas the MO gathered relatively in the lower right region, which was

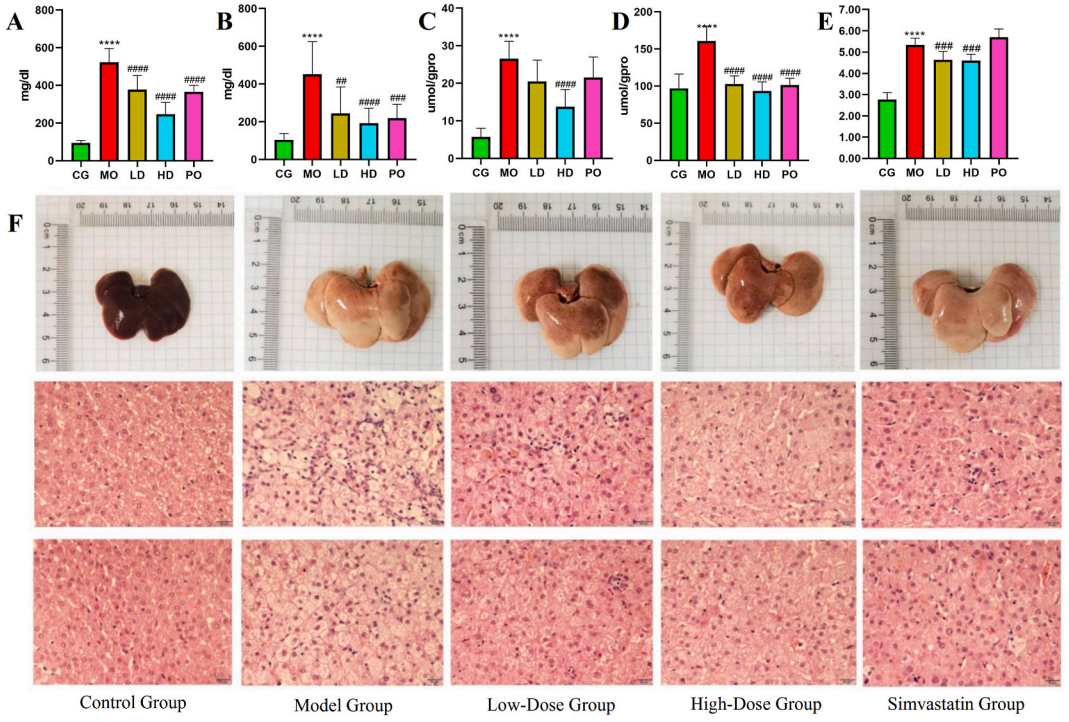

Fig. 2. The pharmacodynamic evaluation of LGZG Decoction. (A) Comparison of serum TC levels; (B) Comparison of serum TG levels; (C) Comparison of liver tissue TC levels; (D) Comparison of liver tissue TG levels; (E) Comparison of liver index; (F) Comparison of pathomorphology between sample groups; **** Compared with CG, $P < 0.0001$; ## Compared with MO, $P < 0.01$; ### Compared with MO, $P < 0.001$; #### Compared with MO, $P < 0.0001$.

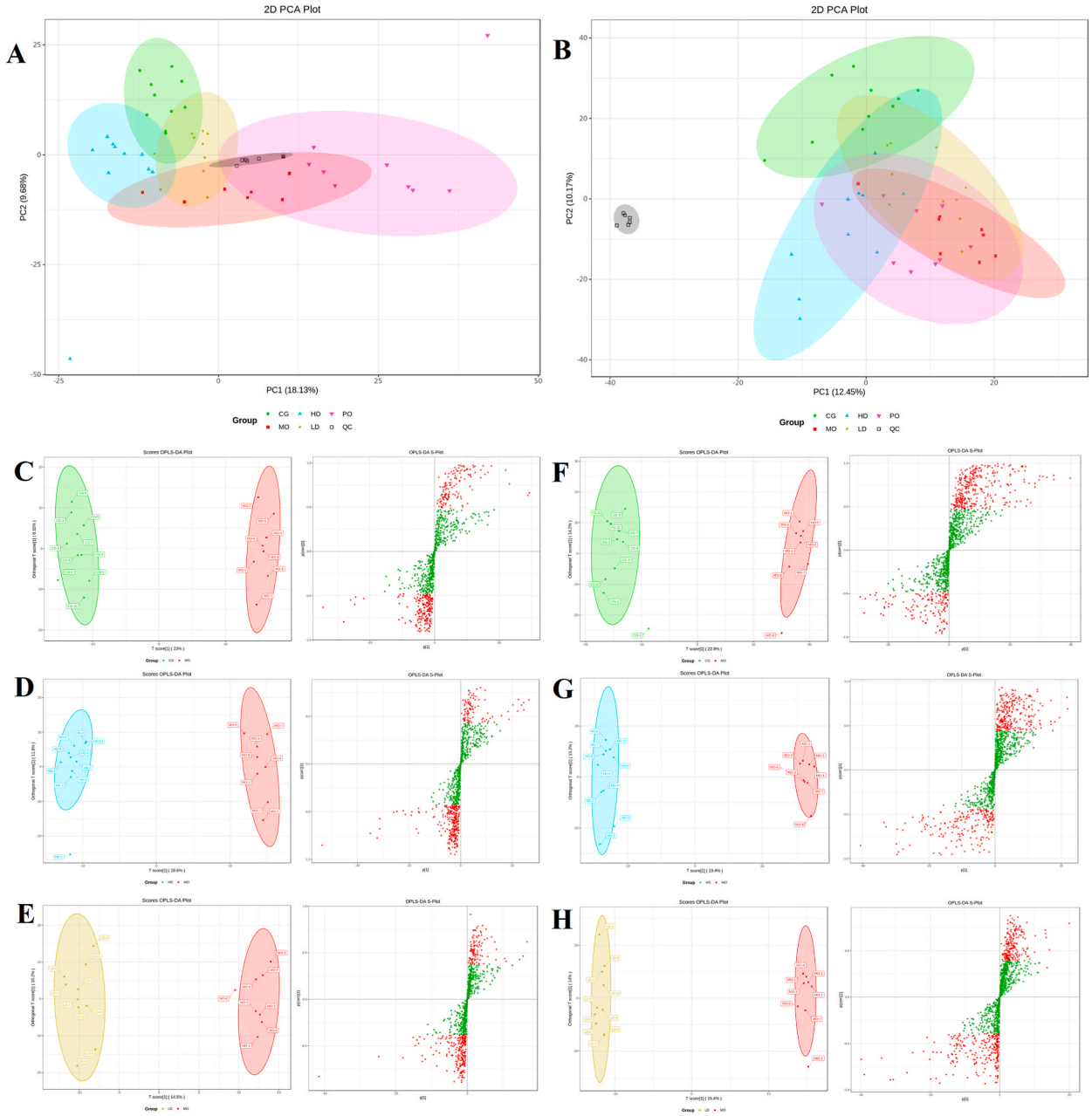

Fig. 3. PCA score plots, OPLS-DA plots and S-plots among samples under the action of LGZG. (A) PCA score plots in positive ion mode; (B) PCA score plots in negative ion mode; (C) CG vs MO results in positive ion mode; (D) HD vs MO results in positive ion mode; (E) LD vs MO results in positive ion mode; (F) CG vs MO results in negative ion mode.; (G) HD vs MO results in negative ion mode; (H) LD vs MO results in negative ion mode.

distinctly different. Similarly, the HD and LD remained clustered between the two, indicating that LGZGD can effectively regress HL metabolite levels.

To further identify the differential metabolites between the groups, OPLS-DA was performed to compare the groups separately. We established OPLS-DA models between the CG and MO, MO and HD, MO and LD. Furthermore, the S-plot curves and 200 permutation tests were performed and plotted to determine whether the model was over-fitted. The Q2 in all groups was larger than 0.808, and the differences between R2Y and Q2 were less than 0.3, which indicated that the fit and predictive ability of the model was excellent. Fig. 3C–H shows the relevant OPLS-DA score plots and S-plot plots. Table S3 presents the predictive parameters between the models.

3.3.2. Results of differential metabolite identification

Based on the OPLS-DA model, metabolites that fulfilled the conditions of FC $\geq$ 1.5 or FC $\leq$ 0.67, VIP $\geq$1 and $P < 0.05$ were screened

to obtain the differential metabolites between groups. For comparison, we listed the results of the comparisons between CG and MO as group 1, MO and HD as group 2, MO and LD as group 3. Finally, 109,79,32 differential metabolites in the positive mode and 223,194,113 in the negative mode were filtered for group 1, group 2, and group 3, respectively. Further analysis revealed that there were 14 and 48 differential metabolites between group 1 and group 2 in positive and negative mode, which contained 3 and 16 metabolites among all three groups, respectively. As all of these 62 metabolites tended to be back-regulated after administration, we selected them as differential metabolites (Fig. 4A and B, Table S4).

We selected 19 metabolites that were co-moderated by the three groups for presentation. In the positive ion mode, three metabolites were involved, namely one amino acid and two glycerophospholipids (GPs); in the negative ion mode, 16 metabolites were contained, namely four amino acids, four GPs, two benzenes and their substituted derivatives, two organic acids and their derivatives, one FA, one alkaloid, one tryptamine, and one hormone. Based on the differences between these 19 differential metabolites, the violin plots were constructed for the CG, MO, LD, HD, and SG for cross-sectional comparison (Fig. 4C). Meanwhile, we performed ROC curve analysis for 19 differential metabolites to verify their accuracy as HL biomarkers, which were shown in Fig. S4 and Table S5.

3.4. Results of quantitative lipidomics analysis

3.4.1. Results of lipid composition analysis

We detected 936 lipids involving 38 subclasses, including 493 GPs, 226 glycerolipids (GLs), 100 FAs, 81 sphingolipids (SPs), 34 sterol lipids (STs), and two prenol lipids (Table S6). Considering the lipid quantities, the top five lipids in the subclasses were TG (191, 20.41 %), phosphatidylcholine (PC, 94, 10.04 %), ether-linked phosphatidyl-ethanolamine (PE-O) (85, 9.08 %), PE (61, 6.52 %) and acylcarnitines (CAR) (53, 5.66 %), and the least represented lipids were cholesterol (one, 0.001 %) and galactolipid monogalactosyldiacylglycerol (one, 0.001 %). We plotted a ring diagram (Fig. S5A), radar chart (Fig. S5B), and histogram (Fig. S5C) separately to further visualize the lipid subclasses and their quantitative compositions. The lipid composition analysis across the five groups showed

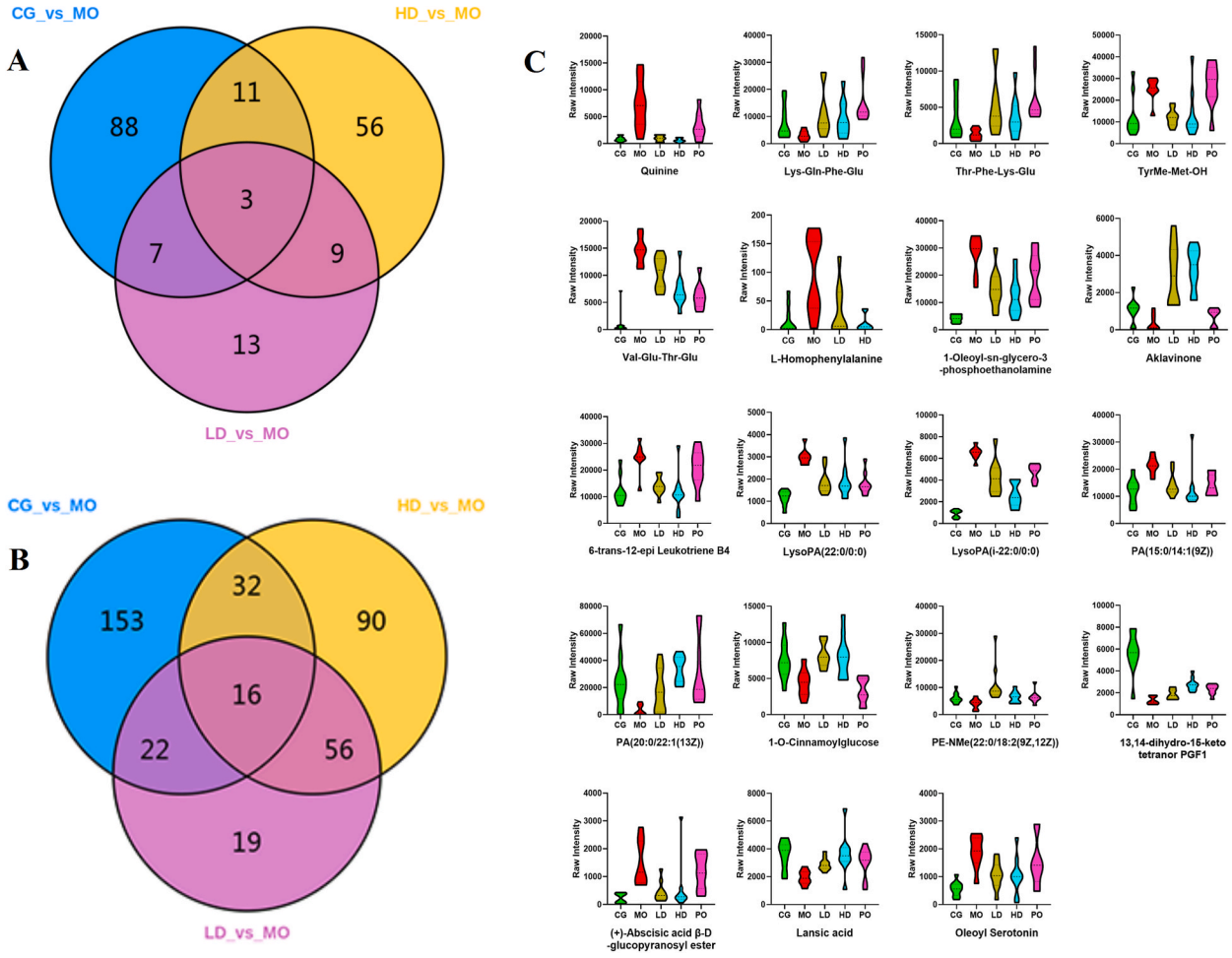

Fig. 4. Analysis of differential metabolites among different groups. (A) Venn diagrams of metabolite among different groups in positive ion mode; (B) Venn diagrams of metabolite among different groups in negative ion mode; (C) Violin plots of 19 metabolites for non-targeted metabolomics.

that lipid compositions were completely identical for all five groups, indicating that HL occurrence is mainly due to differences in lipid contents rather than species (Figs. S5D–O). Please refer to the supplementary material for more details on lipid chain length and unsaturation analysis (Figs. S6–S7).

3.4.2. *Results of multivariate statistical analysis*

PCA and cluster analysis were performed on the samples to observe the separation trend between the samples, which is depicted in Fig. 5A. The PCA results indicated that the CG showed significant intra-group aggregation in the left region, whereas the MO showed the same in the right region. The HD, LD, and SG were located in the middle of the two. The cluster analysis showed that CG and MO metabolite levels were visibly different, which exhibited back-regulation after pharmacological intervention. The OPLS-DA results showed that Q2 values between all groups were larger than 0.767, and differences between R2Y and Q2 were less than 0.3, indicating the excellent fit and predictive ability of the model. Fig. 5B and C shows relevant OPLS-DA score plots and S-plots. Table S7 presents predictive parameters between the models.

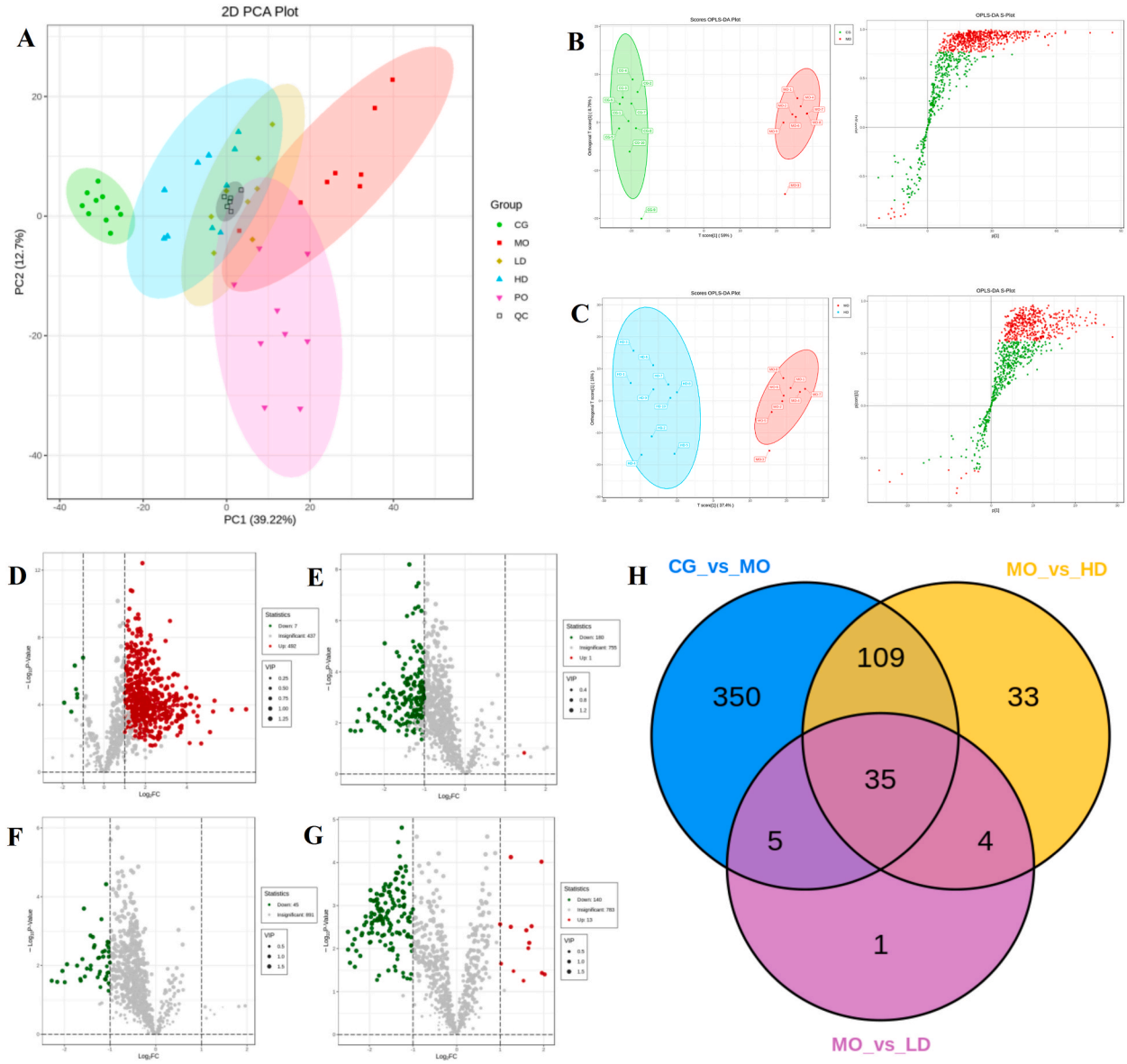

Fig. 5. Results of multivariate statistical analysis and differential metabolite screening in LGZGD. (A) PCA score plots among samples under the action of LGZGD; (B) OPLS-DA plots and S-plots between CG and MO; (C) OPLS-DA plots and S-plots between HD and MO; (D) Volcano plot between CG and MO; (E) Volcano plot between HD and MO; (F) Volcano plot between LD and MO; (G) Volcano plot between SG and MO; (H) Venn diagrams of metabolite among different groups.

3.4.3. Results of the screening of differential lipids

Based on the OPLS-DA model, lipids that met conditions such as FC ≥ 2.0 or FC ≤ 0.5, $P < 0.05$, and VIP ≥1 were screened to obtain differential lipids. Overall, 499 differential lipids were found in group 1, of which 492 were upregulated and seven were downregulated; 181 differential lipids were filtered in group 2, including one upregulated and 180 downregulated lipids; and 45 differential lipids were selected for group 3, and all were downregulated. Further analysis revealed that there were 144 differential lipids between group 1 and group 2, which contained 35 lipids among all three groups. As all 144 metabolites exhibited back-regulation after LGZGD administration, we selected them as differential lipids (Fig. 5D–H, Table S8).

The intersection among the three groups resulted in 35 differential lipids, including 28 GLs (all TG), one FA (CAR), five GPs (two phosphatidic acids (PA), one PC, one lysophosphatidylcholine (LPC), and one PE), and one ST (cholesterol esters). Based on differences in the levels of these 35 differential lipids, violin plots were produced for the CG, MO, LD, HD, and SG for a cross-sectional comparison (Fig. 6). In addition, we also performed ROC curve analysis of these 35 differential lipids, which are presented in Fig. S4 and Table S9.

3.5. Results of network pharmacology and molecular docking

3.5.1. Screening of intersectional targets

Eighty chemical components were identified from LGZGD, with 343 targets as potential targets. For HL targets, 88 were selected from Drugbank, 1969 from Genecard, 55 from OMMI, and 25 from TTD. Following the principle of the relevance score greater than 5 in the Genecard database, while reflecting on other databases, 85 disease targets were identified. Regarding differential metabolites and lipids, 35 metabolites and 86 lipids were selected as priority targets, which were then filtered to obtain 974 relevant targets. By comparing the intersection of the three parts, seven core targets were finally confirmed, namely HMGCR, PPARA, PPARG, PPARD,

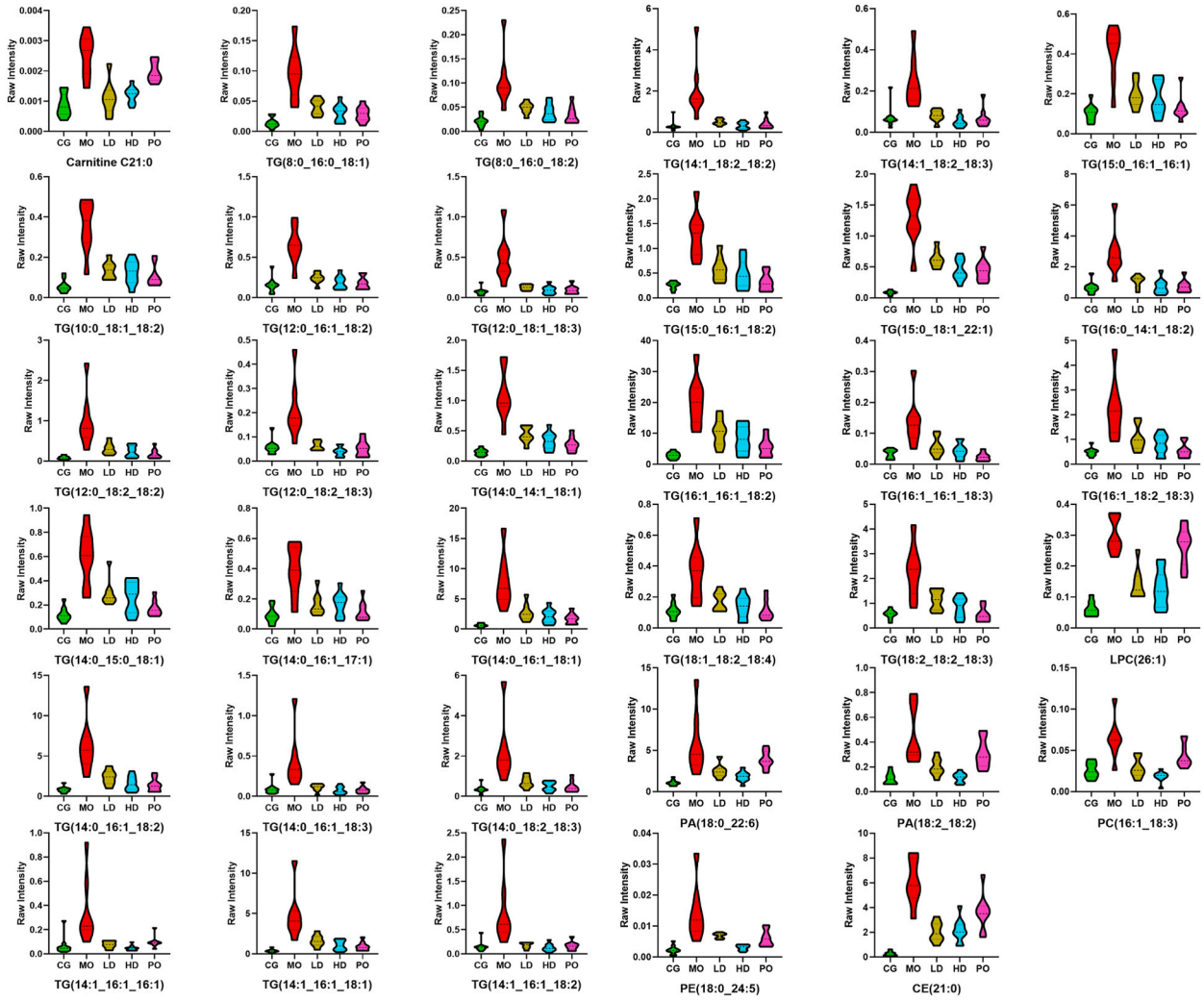

Fig. 6. Violin plot of 35 quantitative lipid comparisons between groups.

CES1, MTTP, and SERPINE1 (Fig. 7A and B).

3.5.2. Results of molecular docking

According to the prediction results, six key components were selected for molecular docking with the core targets, namely genistein, naringenin, quercetin, kaempferol, formononetin, and taxifolin. All binding energies were less than −5.0 kcal/mol, indicating that they exhibited promising binding properties (Fig. 7C–J, Table S10).

4. Discussion

Here, we applied a combination of pharmacodynamic studies, untargeted metabolomics, quantitative lipidomics, network pharmacology, and molecular docking to screen the LGZGD potential mechanism for treating HL. In the pre-study stage of animal model establishment, different experimental animal types were thoroughly investigated. For HL models, animal models that are similar to humans regarding lipoprotein composition and regulation were selected [23]. Large animals, including monkeys and pigs, require

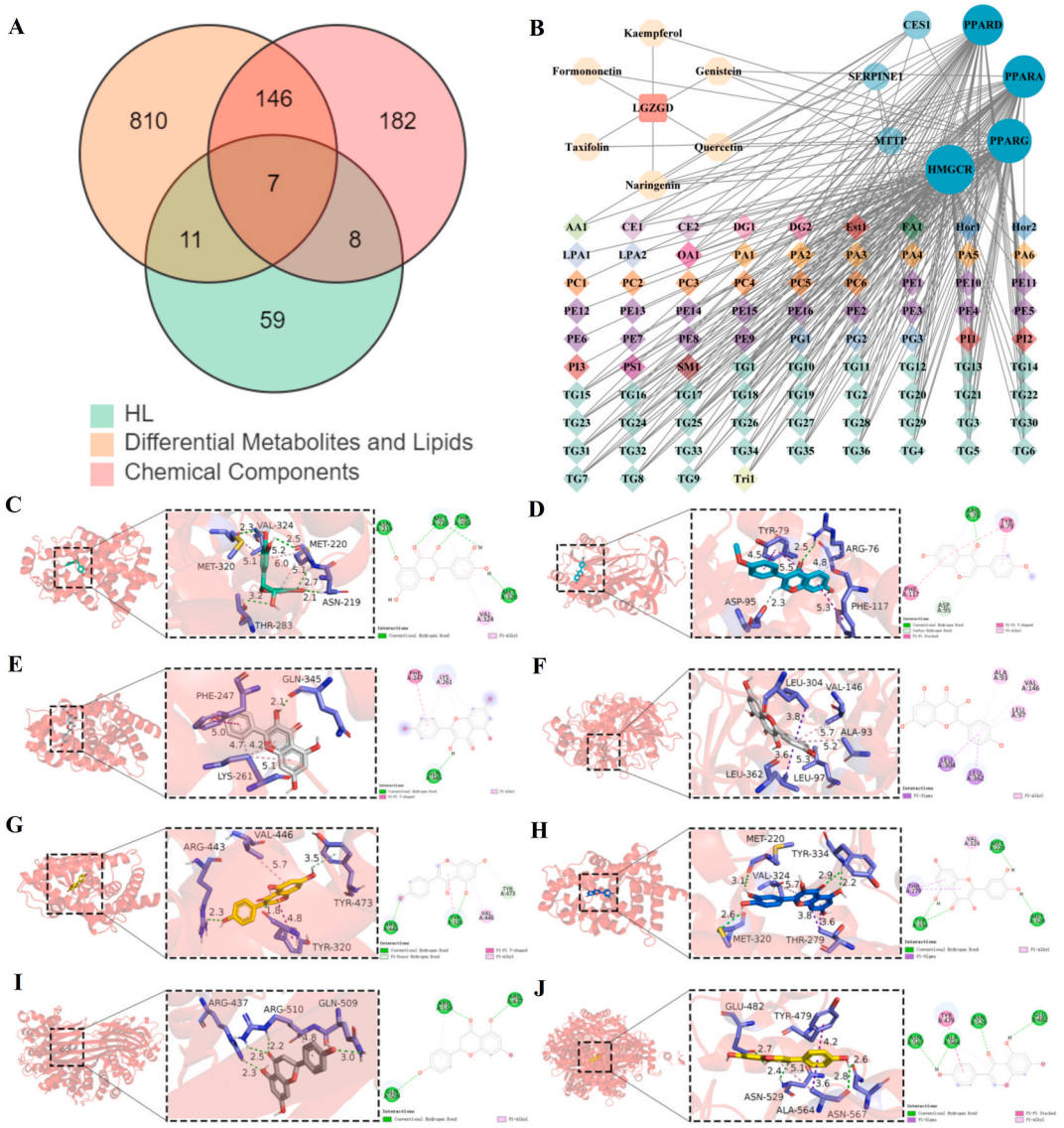

Fig. 7. Results of network pharmacology and molecular docking. (A) Venn diagrams of HL, chemical compositions and differential metabolites; (B) Network diagram of chemical components, targets and differential metabolites; (C) Molecular docking of Taxifolin and PPARA; (D) Molecular docking of Formononetin and SERPINE1; (E) Molecular docking of Kaempferol and PPARG; (F) Molecular docking of Kaempferol and CES1; (G) Molecular docking of Genistein and PPARD; (H) Molecular docking of Quercetin and PPARA; (I) Molecular docking of Naringenin and MTTP; (J) Molecular docking of Genistein and HMGCR.

more time to model, with unstable results and large differences in reproducibility between groups [24,25]. For rats and mice, cholesterol is primarily transported by high-density lipoproteins (HDL). In contrast, the cholesteryl ester transfer protein (CETP) facilitates the transfer of cholesterol esters between different lipoproteins in humans. It not only exchanges cholesterol from HDL to apolipoprotein B-containing lipoproteins, such as low-density lipoproteins (LDL), but also influences the distribution of cholesteryl esters among various lipoproteins, including very-low-density lipoproteins (VLDL) and chylomicron remnants. As HA contains CETP, its lipid metabolism patterns are closer to those of humans, leading to more consistent results with human conditions [26–28]. Therefore, HA was finally selected as an animal model for this study.

Preliminary studies have discovered that 328 different metabolites were present between CG and MO, of which 109 were in the positive and 223 in the negative modes (four metabolites were present in both positive and negative modes), including 91 GP, 41 amino acids and their metabolites, 28 organic acids and their derivatives, 27 benzenes and substituted derivatives, 25 heterocyclic compounds, 18 FAs, 17 GLs, and other metabolites. That is to say, under pathological conditions, the overall levels of various metabolites in the body have been altered, which presumably may lead to a variety of physiological changes, such as alterations in the cell membrane structure and functions, energy supply dysregulation, inflammatory cell accumulation and localized cell apoptosis.

Pharmacodynamic studies indicated that after LGZGD intervention, TC and TG levels in the LD, HD, and SG were significantly regressed, hepatocyte morphology was also improved, inferring that LGZGD has a positive therapeutic effect on HL. The liver index results showed no significant difference between the SG and MO, suggesting that the simvastatin therapeutic effects on HL-induced liver hypertrophy were not significant, and presumably, simvastatin may play a therapeutic role by regulating TC and TG levels.

The non-targeted metabolomics results revealed that the presence of 25 different GP subclasses among 62 differential metabolites changed throughout the experiment, specifically seven lysophosphatidylethanolamines (LPEs), five PCs, four PAs, three lipoproteins (a) (LPAs), three PEs, one PG, one phosphatidylinositol (PI), and one phosphatidylserine (PS), suggesting that the LGZGD mechanism for HL might be closely related to the correction of the lipid metabolic processes. Therefore, quantitative lipidomics studies were further performed to systematically investigate the transformation and metabolic processes of different lipids subclasses. The results showed that 144 different lipids were filtered to obtain 19 subclasses of five major categories, including FA (CAR), GL (DG and TG), GP (PE, PC, PE-P, PI, PA, PG, N-Acyl-LPE, PE-O, PS, LPC, LPE, and PC-O), ST (CE), and SP (Cer, HexCer, and SM).

By the network pharmacological prediction of drug chemistry, HL, differential metabolites, and lipids, we identified seven core targets, namely HMGCR, PPARA, PPARD, PPARG, CES1, MTTP and SERPINE1. The main cholesterol source in humans is its synthesis. HMGCR, the cholesterol biosynthesis rate-limiting enzyme, catalyzes 3-hydroxy-3-methylglutaryl coenzyme A conversion to mevalonate during cholesterol synthesis. Blocking HMGCR can reduce cholesterol synthesis, whereas feedback stimulation can increase the number and activity of LDL receptors in hepatocytes, thus regulating lipid metabolism disorders [29,30]. Currently, popular statins on the market, including simvastatin and atorvastatin, are used as HMGCR inhibitors. Molecular docking results showed that genistein and naringenin bind tightly to HMGCR. Combined with the network pharmacology results, it was inferred that these two components can act on HMGCR to deregulate 70 different metabolites and lipids during cholesterol metabolism, including 36 TGs, and 2 CEs. These TG and CE are transported by chylomicrons and hydrolyzed in the presence of lipoprotein lipase, leading to the release of FA, which can be utilized for energy production or stored. Meanwhile, nascent HDL particles are formed through the binding of ApoA-I to phospholipids and FC. During HDL maturation, FC is converted to CE by lecithin-cholesterol acyltransferase (LCAT), and mature HDL is involved in various lipid metabolism processes, including the reverse cholesterol transport.

The PPAR signaling pathway is a classical lipid-lowering mechanism by participating in FA oxidation, cholesterol synthesis, and metabolism [31]. PPAR can be divided into three subtypes, of which PPARA can be involved in gene expression for lipid metabolism in the liver and skeletal muscle [32], PPARD can participate in lipid oxidation and cell proliferation [33], and PPARG can promote adipocyte differentiation and enhance blood glucose uptake [34]. Here, targets were enriched for all three PPAR subtypes, with PPARA associated with three chemical components and 48 differential metabolites, PPARD related to one chemical component and 45 differential metabolites, and PPARG linked to five chemical components and 52 differential metabolites. Considering that numerous lipid subclasses can be synthesized and transformed, it can be said that LGZGD acts on the PPAR with a wide range of effects, which deserves further detailed mechanism studies.

In addition, CES1, MTTP, and SERPINE1 are also important for lipid metabolism. CES1 can participate in the hydrolysis of cholesterol esters and TG, releasing the FFA and cholesterol for energy production or re-esterification. By hydrolyzing cholesteryl esters, CES1 helps maintain intracellular cholesterol homeostasis, regulates the synthesis of new lipids and maintains cell membrane integrity [35]. MTTP promotes TG synthesis in the endoplasmic reticulum and participates in the assembly of lipoprotein particles, especially VLDL and CM, which indirectly affects VLDL secretion in the liver and participates in cholesterol transport [36,37]. SERPINE1, a serine protease inhibitor, is predominantly recognized for its roles in blood coagulation, tumor biology, and inflammatory responses. While its direct involvement in lipid metabolism remains undocumented, its rs1799889 variant can significantly reduce TC, TG, and LDL-C levels to decrease coronary artery disease risk, suggesting an indirect role for SERPINE1 in interfering with lipid metabolism [38].

There are some shortcomings in this study, such as some samples missing, insufficiently in-depth study of mechanism and insufficient validation. Future studies will be directed towards validating the key components and core targets identified in this work. These will be essential to substantiate our preliminary findings and to elucidate the intricate mechanisms by which TCM like LGZGD can regulate lipid metabolism, thereby advancing the therapeutic potential of TCM in managing metabolic disorders.

5. Conclusion

In conclusion, our study introduces an integrated research approach to preliminarily reveal the protective effects of LGZGD on HL

and elucidate its pharmacodynamic material basis. Through the combined use of LC-MS/MS, multi-omics association analysis, network pharmacology and molecular docking, we have identified potential targets and mechanisms through which LGZGD may exert its effects, which have been predicted to be the initial approximation for the pharmacodynamic substances.

Declaration of ethics

All animal experiments were approved and performed under the relevant regulations of the Experimental Animal Ethics Committee of Hebei Invivo Biotechnology Co. (Approval number SY2021-05). Our research wasperformed in accordance with the ARRIVE guidelines.

Data availability statement

All data supporting the findings of this study are available within the article or its supplementary materials.

Funding

This work was supported by The Natural Science Foundation of Hebei Province under Grant[number H2022423335].

CRediT authorship contribution statement

Baolin Li: Writing – original draft, Methodology, Investigation, Formal analysis, Data curation, Conceptualization. **Qi Qian:** Methodology, Investigation, Formal analysis, Conceptualization. **Liying Niu:** Writing – review & editing, Supervision, Project administration, Funding acquisition, Conceptualization. **Xinguo Wang:** Writing – review & editing, Supervision, Project administration, Funding acquisition, Conceptualization.

Declaration of competing interest

The authors declare that they have no known competing financial interests or personal relationships that could have appeared to influence the work reported in this paper.

Abbreviations

AUC	Area under the curve
CAR	Acyl carnitines
CE	Cholesteryl ester/Collision energy
Cer	Ceramide;
DG	Diacylglycerol
DP	Declustering potential
ESI	Electrospray ionization
FA	Fatty acid
FC	Fold change
GL	Glycerolipid
GP	Glycerophospholipid
HA	hamsters
HL	Hyperlipidaemia
HPLC	High Performance Liquid Chromatography
KEGG	Kyoto encyclopedia of genes and genomes
LGZGD	Lingguizhugan Decoction
LPA	Lysophosphatidic acid
LPC	Lysophosphatidylcholine;
LPE	Lysophosphatidylethanolamine;
LPG	Lysophosphatidylglycerol
LPI	Lysophosphatidylinositol
LPS	Lysophosphatidylserine;
MG	Monoacylglycerol
MRM	Multiple reaction monitoring
MS	Mass spectrometry
OPLS-DA	Orthogonal projection to latent structures-discriminant analysis
PA	Phosphatidic acid
PC	Phosphatidylcholine;
PCA	Principal component analysis

PE Phosphatidylethanolamine;
PG Phosphatidylglycerol
PI Phosphatidylinositol
PS Phosphatidylserine;
QC Quality control
QQQ Triple quadrupoles
ROC Receiver operating characteristic curve
SM Sphingomyelin
SPH Sphingosine;
SP Sphingolipid
ST Sterol lipid
TC Serum total cholesterol
TCM Traditional Chinese Medicine;
TG Triacylglycerol
TIC Total ion chromatogram
TOF Time of flight
VIP Variable importance in projection

Appendix A. Supplementary data

Supplementary data to this article can be found online at https://doi.org/10.1016/j.heliyon.2024.e35426.

References

[1] L.A. Giles, Hyperlipidemia prevention and management utilizing lifestyle changes, J. Midwifery Wom. Health 69 (3) (2024) 361–369, https://doi.org/10.1111/jmwh.13637.
[2] S. Fischer, U. Schatz, U. Julius, Practical recommendations for the management of hyperlipidemia, Atherosclerosis Suppl. 18 (2015) 194–198, https://doi.org/10.1016/j.atherosclerosissup.2015.02.029.
[3] M. Ruscica, N. Ferri, M. Banach, C.R. Sirtori, A. Corsini, Side effects of statins: from pathophysiology and epidemiology to diagnostic and therapeutic implications, Cardiovasc. Res. 118 (17) (2023) 3288–3304, https://doi.org/10.1093/cvr/cvac020.
[4] H. Zhang, S. Li, Y. Feng, Q. Zhang, B. Xie, Efficacy of fibrates in the treatment of primary biliary cholangitis: a meta-analysis, Clin. Exp. Med. 23 (5) (2022) 1741–1749, https://doi.org/10.1007/s10238-022-00904-2.
[5] A. Kei, T.D. Filippatos, M.S. Elisaf, The safety of ezetimibe and simvastatin combination for the treatment of hypercholesterolemia, Expet Opin. Drug Saf. 15 (4) (2016) 559–569, https://doi.org/10.1517/14740338.2016.1157164.
[6] S. Li, T.H. So, G. Tang, H.Y. Tan, N. Wang, B.F.L. Ng, C.K.W. Chan, E.C. Yu, Y. Feng, Chinese herbal medicine for reducing chemotherapy-associated side-effects in breast cancer patients: a systematic review and meta-analysis, Front. Oncol. 10 (2020) 599073, https://doi.org/10.3389/fonc.2020.599073.
[7] L. Deng, X. Zhou, Z. Lan, K. Tang, X. Zhu, X. Mo, Z. Zhao, Z. Zhao, M. Wu, Simotang alleviates the gastrointestinal side effects of chemotherapy by altering gut microbiota, J Microbiol Biotechn 32 (4) (2022) 405–418, https://doi.org/10.4014/jmb.2110.10018.
[8] X. Li, G. Xu, S. Wei, B. Zhang, H. Yao, Y. Chen, W. Liu, B. Wang, J. Zhao, Y. Gao, Lingguizhugan decoction attenuates doxorubicin-induced heart failure in rats by improving TT-SR microstructural remodeling, BMC Compl. Alternative Med. 19 (1) (2019) 360, https://doi.org/10.1186/s12906-019-2771-6, 2019.
[9] Y. Dang, S. Hao, W. Zhou, L. Zhang, G. Ji, The traditional Chinese formulae Ling-gui-zhu-gan decoction alleviated non-alcoholic fatty liver disease via inhibiting PPP1R3C mediated molecules, BMC Compl. Alternative Med. 19 (1) (2019) 8, https://doi.org/10.1186/s12906-018-2424-1.
[10] M. Liu, Y. Huang, T. Zhang, L. Tan, X. Lu, J. Qin, Lingguizhugan decoction attenuates diet-induced obesity and hepatosteatosis via gut microbiota, World J. Gastroenterol. 25 (27) (2019) 3590–3606, https://doi.org/10.3748/wjg.v25.i27.3590.
[11] S. Xiang, J. Zhao, Y. Lu, R. Chen, Y. Wang, Y. Chen, B. Long, L. Zhu, P. Yao, Y. Xu, et al., Network pharmacology-based identification for therapeutic mechanism of Ling-Gui-Zhu-Gan decoction in the metabolic syndrome induced by antipsychotic drugs, Comput. Biol. Med. 110 (2019) 1–7, https://doi.org/10.1016/j.compbiomed.2019.05.007.
[12] B. Li, S. Fan, J. Hu, Y. Ma, Y. Feng, F. Wang, X. Wang, L. Niu, Phytochemical analysis using UPLC-MS/MS combined with network pharmacology methods to explore the biomarkers for the quality control of lingguizhugan decoction, Evid Based Complement Alternat Med 12 (2021) 7849032, https://doi.org/10.1155/2021/7849032.
[13] X. Wang, Y. Gao, J. Zhang, H. Zhang, S. Sun, S. Su, D. Kong, Q. Wang, Revealment study on the regulation of lipid metabolism by Lingguizhugan Decoction in heart failure treatment based on integrated lipidomics and proteomics, Biomed. Pharmacother. 158 (2022) 114066, https://doi.org/10.1016/j.biopha.2022.114066.
[14] M. Zhu, X. Wang, K. Wang, Z. Zhao, Y. Dang, G. Ji, F. Li, W. Zhou, Lingguizhugan decoction improves non-alcoholic steatohepatitis partially by modulating gut microbiota and correlated metabolites, Front. Cell. Infect. Microbiol. 13 (2023) 1066053, https://doi.org/10.3389/fcimb.2023.1066053.
[15] L. Zhao, S. Wang, X. Xu, W. Guo, J. Yang, Y. Liu, S. Xie, G. Piao, T. Xu, Y. Wang, et al., Integrated metabolomics and network pharmacology to reveal the lipid-lowering mechanisms of Qizha Shuangye granules in hyperlipidemic rats, J. Sci. Food Agric. 104 (6) (2023) 3265–3274, https://doi.org/10.1002/jsfa.13213.
[16] W. Gao, M. Tian, M. Li, S. Gao, X. Wei, C. Gao, Y. Zhou, T. Li, H. Wang, B. Bian, et al., Study on the potential mechanism of Qingxin Lianzi Yin Decoction on renoprotection in db/db mice via network pharmacology and metabolomics, Phytomedicine 126 (2023) 155222, https://doi.org/10.1016/j.phymed.2023.155222.
[17] X.Y. Chua, F. Torta, J.R. Chong, N. Venketasubramanian, S. Hilal, M.R. Wenk, C.P. Chen, T.V. Arumugam, D.R. Herr, M.K.P. Lai, Lipidomics profiling reveals distinct patterns of plasma sphingolipid alterations in Alzheimer's disease and vascular dementia, Alzheimer's Res. Ther. 15 (1) (2023) 214, https://doi.org/10.1186/s13195-023-01359-7.
[18] T. Zhao, Q. Yan, C. Wang, J. Zeng, R. Zhang, H. Wang, L. Pu, X. Dai, H. Liu, L. Han, Identification of serum biomarkers of ischemic stroke in a hypertensive population based on metabolomics and lipidomics, Neuroscience 533 (2023) 22–35, https://doi.org/10.1016/j.neuroscience.2023.09.017.
[19] X. Yang, C. Chi, W. Li, Y. Zhang, S. Yang, R. Xu, R. Liu, Metabolomics and lipidomics combined with serum pharmacochemistry uncover the potential mechanism of Huang-Lian-Jie-Du decoction alleviates atherosclerosis in ApoE-/- mice, J. Ethnopharmacol. 324 (2024) 117748, https://doi.org/10.1016/j.jep.2024.117748.

[20] V. Caponigro, A.L. Tornesello, F. Merciai, D. La Gioia, E. Salviati, M.G. Basilicata, S. Musella, F. Izzo, A.S. Megna, L. Buonaguro, et al., Integrated plasma metabolomics and lipidomics profiling highlights distinctive signature of hepatocellular carcinoma in HCV patients, J. Transl. Med. 21 (1) (2023) 918, https://doi.org/10.1186/s12967-023-04801-4.
[21] S. Zhao, J. Zhang, Y. Chen, X. Cui, H. Liu, Y. Yan, Y. Sun, Y. Qi, Y. Liu, The comprehensive mechanism underlying Schisandra polysaccharide in AD-like symptoms of Aβ25-35-induced rats based on hippocampal metabolomics and serum lipidomics techniques, J Pharmaceut Biomed. 236 (2023) 115717, https://doi.org/10.1016/j.jpba.2023.115717.
[22] M. Kanehisa, S. Goto, KEGG: kyoto encyclopedia of genes and genomes, Nucleic Acids Res. 28 (1) (2000) 27–30, https://doi.org/10.1093/nar/28.1.27.
[23] Z.A. Rizvi, R. Dalal, S. Sadhu, A. Binayke, J. Dandotiya, Y. Kumar, T. Shrivastava, S.K. Gupta, S. Aggarwal, M.R. Tripathy, et al., Golden Syrian hamster as a model to study cardiovascular complications associated with SARS-CoV-2 infection, Elife 11 (2022), https://doi.org/10.7554/eLife.73522.
[24] A. Trollope, J.V. Moxon, C.S. Moran, J. Golledge, Animal models of abdominal aortic aneurysm and their role in furthering management of human disease, Cardiovasc. Pathol. 20 (2) (2010) 114–123, https://doi.org/10.1016/j.carpath.2010.01.001.
[25] N.V. Mushenkova, V.I. Summerhill, Y.Y. Silaeva, A.V. Deykin, A.N. Orekhov, Modelling of atherosclerosis in genetically modified animals, Am J Transl Res 11 (8) (2019) 4614–4633.
[26] X. Lin, P. Ma, C. Yang, J. Wang, K. He, G. Chen, W. Huang, J. Fan, X. Xian, P. Wang, et al., Dietary-induced elevations of triglyceride-rich lipoproteins promote atherosclerosis in the low-density lipoprotein receptor knockout Syrian golden hamster, Front Cardiovasc Med 8 (2021) 738060, https://doi.org/10.3389/fcvm.2021.738060.
[27] V. Suresh, R. Sundaram, P. Dash, S.C. Saba, D. Mohapatra, S. Mohanty, D. Vasudevan, S. Senapati, Macrophage migration inhibitory factor of Syrian golden hamster shares structural and functional similarity with human counterpart and promotes pancreatic cancer, Sci. Rep. 9 (1) (2019) 15507, https://doi.org/10.1038/s41598-019-51947-7.
[28] E. Avolio, G. Fazzari, M. Zizza, L. De, R. Di, R. Alò, R. Facciolo, M. Canonaco, Probiotics modify body weight together with anxiety states via pro-inflammatory factors in HFD-treated Syrian golden hamster, Behav. Brain Res. 356 (2018) 390–399, https://doi.org/10.1016/j.bbr.2018.09.010.
[29] B. Scharinger, B. Messner, A. Türkcan, D. Schuster, A. Vuorinen, F. Pitterl, K. Heinz, K. Arnhard, G. Laufer, M. Grimm, et al., Leoligin, the major lignan from Edelweiss, inhibits 3-hydroxy-3-methyl-glutaryl-CoA reductase and reduces cholesterol levels in ApoE-/- mice, J. Mol. Cell. Cardiol. 99 (2016) 35–46, https://doi.org/10.1016/j.yjmcc.2016.08.003.
[30] X. Lu, X. Shi, A. Hu, J. Wang, Y. Ding, W. Jiang, M. Sun, X. Zhao, J. Luo, W. Qi, et al., Feeding induces cholesterol biosynthesis via the mTORC1-USP20-HMGCR axis, Nature 588 (7838) (2020) 479–484, https://doi.org/10.1038/s41586-020-2928-y.
[31] E. Robinson, D.J. Grieve, Significance of peroxisome proliferator-activated receptors in the cardiovascular system in health and disease, Pharmacol. Therapeut. 122 (3) (2009) 246–263, https://doi.org/10.1016/j.pharmthera.2009.03.003.
[32] Z. Chen, X. Sun, X. Li, N. Liu, Oleoylethanolamide alleviates hyperlipidaemia-mediated vascular calcification via attenuating mitochondrial DNA stress triggered autophagy-dependent ferroptosis by activating PPARα, Biochem. Pharmacol. 208 (2022) 115379 https://doi.org/10.1016/j.bcp.2022.115379.
[33] F. Karpe, E.E. Ehrenborg, PPARdelta in humans: genetic and pharmacological evidence for a significant metabolic function, Curr. Opin. Lipidol. 20 (4) (2009) 333–336, https://doi.org/10.1097/MOL.0b013e32832dd4b1.
[34] Y. Huan, X. Pan, J. Peng, C. Jia, S. Sun, G. Bai, X. Wang, T. Zhou, R. Li, S. Liu, et al., A novel specific peroxisome proliferator-activated receptor γ (PPARγ) modulator YR4-42 ameliorates hyperglycaemia and dyslipidaemia and hepatic steatosis in diet-induced obese mice, Diabetes Obes Metab 21 (11) (2019) 2553–2563, https://doi.org/10.1111/dom.13843.
[35] L. Mangum, A. Borazjani, J. Crow, M. Ross, Bioactive lipid metabolism by carboxylesterase 1 (CES1) in macrophages (LB154), Faseb. J. 28 (S1) (2014), https://doi.org/10.1096/fasebj.28.1_supplement.lb154.
[36] H. Ding, J.H. Yu, G. Ge, Y.Y. Ma, J.C. Wang, J. Zhang, J. Liu, RASAL2 deficiency attenuates hepatic steatosis by promoting hepatic VLDL secretion via the AKT/TET1/MTTP Axis, J Clin Transl Hepato 11 (2) (2022) 261–272, https://doi.org/10.14218/JCTH.2022.00042.
[37] X. Dong, J. Wang, M. Zhao, X. Du, H. Fan, Y. Fu, Z. Gong, S. Miao, Betaine alleviates high-fat diet induced excessive lipid deposition in gibel carp hepatopancreas and L8824 cells by enhancing VLDL secretion through HNF4α/MTTP pathway, Aquacult. Nutr. 1 (2024) 8886237, https://doi.org/10.1155/2024/8886237.
[38] Z. Luo, Y. Liu, H. Li, Y. Zhou, Y. Peng, X. Lin, Y. Fang, J. Wan, B. Wei, Systematic review and meta-analysis of SERPINE1 4G/5G insertion/deletion variant with circulating lipid levels, Front Cardiovasc Med 9 (2022) 859979, https://doi.org/10.3389/fcvm.2022.859979.